Leino, Mikko K.; Montoya Moreno, Resti; Ala-Laurinaho, Juha; Valkonen, Risto; Viikari, Ville

# Waveguide-Based Phased Array with Integrated Element-Specific Electronics for 28 GHz

*Published in:*
IEEE Access

*DOI:*
10.1109/ACCESS.2019.2925458

Published: 01/01/2019

*Document Version*
Publisher's PDF, also known as Version of record

*Please cite the original version:*
Leino, M. K., Montoya Moreno, R., Ala-Laurinaho, J., Valkonen, R., & Viikari, V. (2019). Waveguide-Based Phased Array with Integrated Element-Specific Electronics for 28 GHz. *IEEE Access*, *7*, 90045-90054. Article 8746998. https://doi.org/10.1109/ACCESS.2019.2925458

IEEE Access
Multidisciplinary | Rapid Review | Open Access Journal

Received May 31, 2019, accepted June 23, 2019, date of publication June 27, 2019, date of current version July 23, 2019.

*Digital Object Identifier 10.1109/ACCESS.2019.2925458*

# Waveguide-Based Phased Array With Integrated Element-Specific Electronics for 28 GHz

**MIKKO K. LEINO[1], (Student Member, IEEE), RESTI MONTOYA MORENO[1], JUHA ALA-LAURINAHO[1], RISTO VALKONEN[2], AND VILLE VIIKARI[1], (Senior Member, IEEE)**

[1]Department of Electronics and Nanosciences, Aalto University School of Electrical Engineering, 00076 Aalto, Finland
[2]Nokia Bell Labs, Nokia, 00045 Espoo, Finland

Corresponding author: Mikko K. Leino (mikko.k.leino@aalto.fi)

This work was supported by the Nokia Bell Labs. The work of M. K. Leino was supported by the Walter Ahlström Foundation.

**ABSTRACT** Scalable and beam-steerable phased antenna array prototype for the wireless backhaul communication is presented for the 28 GHz. The 16-element phased array consists of low-loss waveguide power division network, waveguide-to-PCB transitions, phase shifters on PCB, and horn antenna elements fed from the PCB. The paper presents a state-of-the-art design where the electronically controlled phase shifters are implemented on the PCB right in the immediate proximity of the radiating elements. Thus, the transmission losses are kept as low as possible, even though each element has their specific PCB-mounted electronics. The design is scalable so that element-specific parts on the PCB do not consume more area than the antenna element. Furthermore, novel matching steps with easy manufacturing are presented in the power division network. The simulated and measured results show good agreement. The measurement results show that the grating-lobe free beam-steering range is $\pm 20^{\circ}$ in both azimuth and elevation. The measured antenna gain at broadside is 11.3 dBi after element phase adjustment, and the majority of the losses are due to the implemented electronics, i.e., the phase shifters.

**INDEX TERMS** 5G, phased arrays, beam steering, phase shifters, power dividers, waveguide transitions.

## I. INTRODUCTION

Global mobile data traffic is predicted to increase 46% annually between 2017 and 2022, mainly due to increased video streaming, and by 2022 smartphone traffic will exceed PC traffic [1]. The existing mobile networks cannot meet the capacity demands of the increasing data traffic.

Therefore, the fifth generation mobile communication networks (5G) have been intensively developed during the past few years [2] and the new standardized systems are expected to come into use by 2020. Generally accepted ways to increase the capacity and lower the latency include wider spectral band, denser networks with more cells, and higher spectral efficiency [3]–[6]. More spectrum and wider bandwidths are available at frequencies higher than those conventionally used for mobile communications.

Millimeter-wave frequencies such as 28, 38, 60 GHz, and 71–76/81–86 GHz (E-band) have been proposed to be used in 5G communications [6]. However, at the proposed millimeter-wave frequencies, the intrinsically high free space propagation loss needs to be compensated with highly directive antennas. Further, lower latencies necessitate denser network which consequently result into great number of base stations needed. Due to these reasons, base stations and their antennas need to be inexpensive, low-power, and small in size for discrete installation. In addition, the new networks should support wireless backhauling, as the wired connections to the antennas would restrict the installation and be costly. The requirements and challenges for wireless millimeter-wave backhauling are discussed in [7].

The high efficiency necessitates that the radiated power by the backhaul antenna is appropriately directed to the 5G access points and base stations. Therefore, the beam direction must be reconfigurable so that it can focus capacity where it is required. Furthermore, high antenna gain is required to maximize the range [8].

The electrical beam steering at mm-waves can be facilitated in several ways: e.g., with beam switching networks, reconfigurable high impedance surfaces, phase shifting, and time-delay networks. Several antenna types with electrical beam steering have been proposed. These include: integrated

The associate editor coordinating the review of this manuscript and approving it for publication was Mohammad Zia Ur Rahman.

  

lens antennas [9], passive beam-forming networks like the Rotman lens [10], leaky wave antennas [11], reconfigurable reflectarrays [12], [13], and phased arrays [14]. The mentioned antennas have been studied extensively and only a limited number of the studies are referenced. However, none of these solutions can simultaneously offer all the desired features like low profile, beam steering in 2-D, high efficiency, and high gain.

The beam of an antenna array can be steered by separately controlling the phase of each array element. Phase shifters can be utilized for this, but they are often mounted on the printed circuit boards (PCB) and at higher frequencies the traditional transmission lines on PCB are prone to heavy losses. For example, a planar realization with element-specific electronics and beam-steering capabilities at 28 GHz have been presented in [15] and [16], and while the performances are otherwise very good, the transmission losses are high.

To avoid great transmission losses, the transmission lines and antenna elements could be designed to be waveguide-based as e.g. in [17]. Other possibility to make antennas with efficient transmission could be by utilizing gap waveguides [18], [19] or substrate integrated waveguides [20], [21].

One potential antenna array for 5G backhaul links has been previously presented for E-band in [22]. In this type of an array, the phase shifters are mounted on the PCB near the antenna elements, and the transmission lines and antenna elements are waveguide-based. This results in a low-loss antenna design that requires compact transitions between the waveguide structures and the PCB. However, the previously presented E-band antenna array has fixed phase shifters and thus the beam steering is not immediate. In this paper, we present an antenna array with electronically controlled phase shifters that can be used to steer the beam in real-time.

The antenna presented in the following is designed to operate at an important 26–30 GHz 5G band. The utilized phase shifters are commercially available and the antenna can be fed with regular WR-28 waveguide. The presented antenna is scalable in a way that the number of elements can be easily increased as the element-specific phase shifter is fitted on the same area on the PCB that the antenna element occupies. In addition, the antenna has potentially low losses, low profile, wide beam-steering range, and high gain. To the authors' knowledge this is the first realization of an antenna where a low-loss power division network and antenna elements are integrated with PCB-mounted, electronically configurable, element-specific integrated circuit components that can be controlled in real time.

Furthermore, this antenna array improves the previously presented power division network by introducing novel matching steps inside it. The introduced steps can be easily fabricated with milling or 3D-printing and they provide simulated reflection coefficient less than -18.5 dB for the whole band. Only limitation for this waveguide-based antenna is that the element spacing is more than $\lambda/2$ at the observed frequency band, e.g., $0.74\lambda$ at 28 GHz. This limitation is dictated by the waveguide size in H-plane that is required for the correct cut-off frequency and thus it cannot be reduced.

The rest of the paper is organized as follows: Section II explains the antenna design in detail, Section III presents the measurement results, and Section IV discusses the future improvements and capabilities of the antenna. Finally, the paper is concluded in Section V.

## II. ANTENNA COMPONENTS

The presented antenna has four main parts: the waveguide-based power division network, waveguide-to-PCB transitions, the PCB on which the electronically controlled phase shifters are embedded, and horn antenna elements. These parts are discussed in detail in the following. The waveguide parts, as well as all the parts of the horn antenna prototype are manufactured from brass by milling. 3D-printing or plastic injection molding could be considered in mass production. Manufactured antenna with element numbering and antenna orientation is presented in Fig. 1.

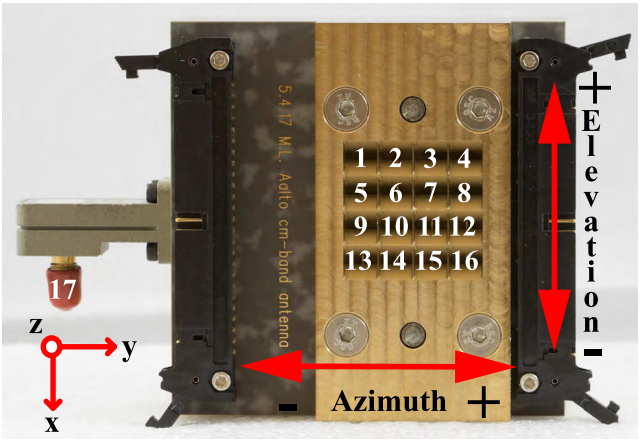


**FIGURE 1.** Manufactured antenna with element numbering and antenna orientation.

### A. POWER DIVISION NETWORK

Power division network provides uniform signal strength for each phase shifter. It consists of two separate parts: the primary and secondary part. The primary network is presented in Fig. 2a and the secondary one in Fig. 2b. Table 1 lists the optimized dimensions for the both structures. Both parts divide the incoming wave to four branches. However, the main difference between two power division networks is that in the primary divider, the electromagnetic wave is divided in E-plane, whereas in the secondary one it is divided in H-plane. For each output of the primary network, there is a secondary network, i.e. the power division network is constructed from one primary network and from four secondary networks. Thus, the single input is divided equally in power to 16 antenna elements.

The primary power division network is basically constructed from several consecutive T-junctions. The matching of the T-junctions is usually done with matching pins, ridges

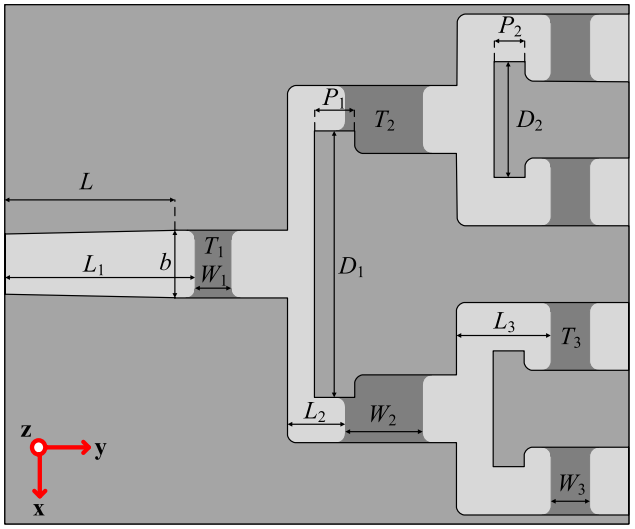


(a)

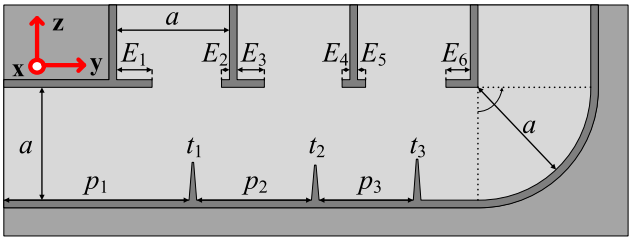


(b)

**FIGURE 2.** Feeding network: (a) primary divider, (b) secondary divider.

**TABLE 1.** Optimized dimensions of the waveguide power division network (All dimensions are in mm).

| $a$ | $b$ | $D_1$ | $D_2$ | $L_1$ | $L_2$ | $L_3$ | $P_1$ | $P_2$ |
|---|---|---|---|---|---|---|---|---|
| 7.40 | 3.70 | 14.84 | 6.09 | 11.08 | 3.15 | 5.10 | 2.27 | 1.72 |
| $W_1$ | $W_2$ | $W_3$ | $T_1$ | $T_2$ | $T_3$ | $p_1$ | $p_2$ | $p_3$ |
| 1.90 | 4.20 | 2.10 | 0.79 | 0.67 | 0.72 | 12.15 | 7.53 | 6.18 |
| $t_1$ | $t_2$ | $t_3$ | $E_1$ | $E_2$ | $E_3$ | $E_4$ | $E_5$ | $E_6$ |
| 2.48 | 2.30 | 2.69 | 2.33 | 0.50 | 1.80 | 0.50 | 0.54 | 1.59 |

or both as reported in [23]. However, these pins might be infeasible due to the manufacturing limitations. To overcome this problem, the novel matching steps are introduced: three different type of steps with varying heights ($T_1$–$T_3$) and lengths ($W_1$–$W_3$) are used to match the single input branch for two outputs and thus reduce the reflections back to the input. Unfortunately, using the matching steps in the secondary network is not possible due to the design architecture, and the matching there is done utilizing matching ridges ($t_1$–$t_3$) and varying slot sizes ($E_1$–$E_6$) for output branches.

Antenna is fed with an HP R281A coaxial-to-waveguide transition connector (2.4 mm coaxial to WR-28 waveguide). Hence, a short transition, ($L = 10$ mm) where the waveguide dimensions are narrowed to match the adapter, is required before the primary feeding network. Note that the waveguide dimensions used elsewhere in the antenna do not exactly match with those of WR-28.

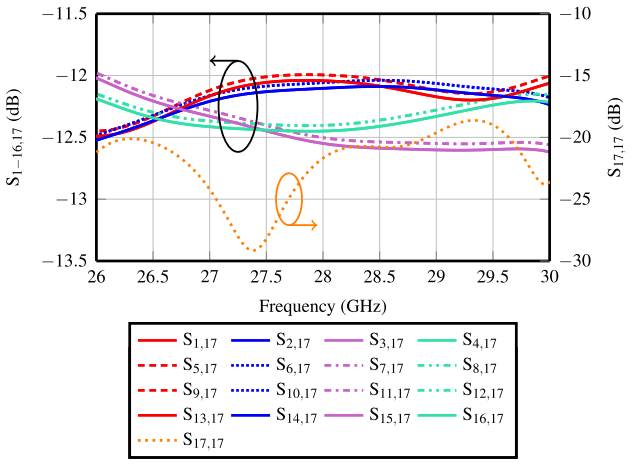


**FIGURE 3.** Simulated S-parameters of the power division network. Structure is fed from port 17.

The simulated S-parameter results are shown in Fig. 3. As the input signal is divided for 16 antennas uniformly, each antenna should have ideally −12 dB transmission coefficient. The simulations show that this is achieved fairly well and the power division network has quite stable performance over the observed frequency band with transmission coefficient varying from −11.9 dB to −12.6 dB. Furthermore, because there are small differences in the secondary network outputs, the results differ from each other slightly. In addition, it can be seen that the elements fed from the same branch of the secondary network, e.g. the elements 1, 5, 9, and 13, have similar performance as expected. These elements have also the same initial phase before phase shifter adjustment which differs from the other branches - the initial phase of each branch is affected by the different electrical lengths in the secondary divider. Furthermore, because the primary network outputs are not completely identical, the elements do not have completely identical transmission coefficients. This is because the innermost outputs differ from the outer ones slightly. Thus, the innermost elements and the outermost have identical results with themselves, e.g. elements 1 and 13 have identical performance, so do elements 5 and 9, etc.

### B. WAVEGUIDE-TO-PCB TRANSITIONS

The feeding network and the horn antenna are based on the rectangular waveguide (RWG). The phase shifters are IC elements to be mounted on a multilayer PCB, thus the transitions are required from the waveguide to the PCB and from the PCB to the antenna. For the sake of simplicity, the microstrip line is chosen to be used as a transmission line structure on PCB over the other planar transmission line structures. Transitions utilizing the microstrip line as a probe in the rectangular waveguide have been researched and they are commonly used, see e.g., [24], [25]. The main goal is to design maximally efficient transitions with the simplest microstrip-line structure possible.

The transition outlines from the side are presented in Fig. 4 and from the top in Fig. 5. Basically, there are two transitions

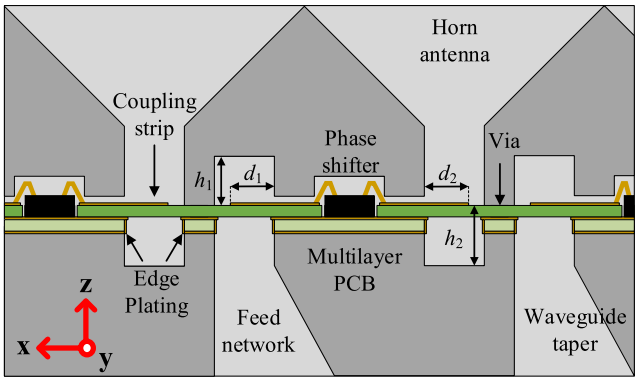


**FIGURE 4.** Side view of the transition structure.

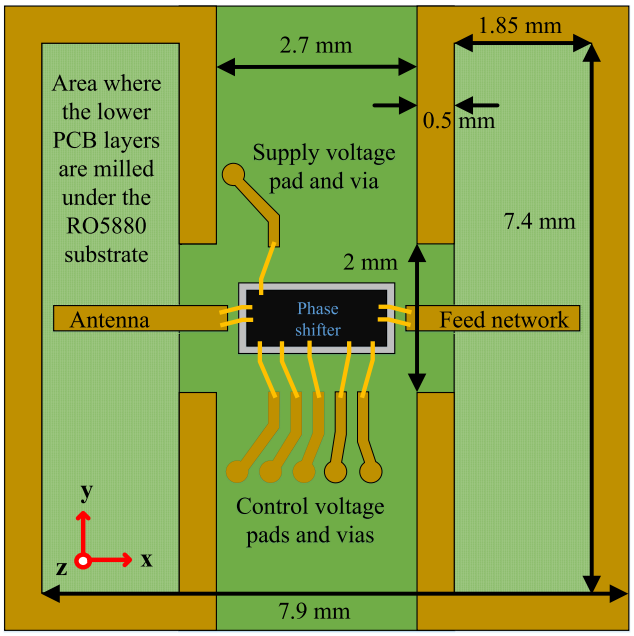


**FIGURE 5.** Top view of the transition structure.

in one element branch. The inbound signal is fed through the RWG and coupled to a microstrip probe that continues as the microstrip line on the PCB. The phase is adjusted on the PCB by the corresponding phase shifter and, thereafter, the signal is transferred to the horn antenna by coupling the microstrip line to the RWG feed of the antenna with the microstrip probe.

The rectangular waveguides in both transitions are identical in dimensions and material. Waveguides are also shorted at both transitions. Essentially, both transitions and their operation principles are very similar with an exception that the probe is on the shorted side in the first transition and on the open waveguide side in the second transition. Subsequently, the electric field must propagate through the substrate in the first transition from the feeding network to the PCB which is not necessary in the second transition where the main part of the field can couple straight to the antenna output. Thus, the transitions have different parameter values when their performance is optimized. Of the several parameters affecting the transitions, the microstrip length inside the waveguide $d_1 = 1.66$ mm and $d_2 = 1.62$ mm and the microstrip distance from the shorted end of the waveguide $h_1 = 1.25$ mm and $h_2 = 1.85$ mm are the most sensitive ones. A sensitivity analysis is performed to these parameters. $d_1$ and $d_2$ can vary about $\pm 60$ $\mu$m and $h_1$ and $h_2$ can vary about $\pm 100$ $\mu$m from the optimized values without affecting to the overall transition performance more than $-0.4$ dB.

To further improve the transition, the part of the PCB that is left inside the waveguide is cut away except the RF-substrate. Thus, a cavity is formed underneath the PCB. Moreover, the cavity is edge-plated with metal to ensure electrical connection through the structure. Except the cavity, the rest of the lowest layer of the PCB is metallized so the waveguides of feeding network part are properly connected to it. With the metal-plated cavities and the vias in the substrate, the waveguide structures can remain continuous and in galvanic connection through the whole structure. Furthermore, this ensures that the electromagnetic field is well confined and not leaked to adjacent branch through the PCB.

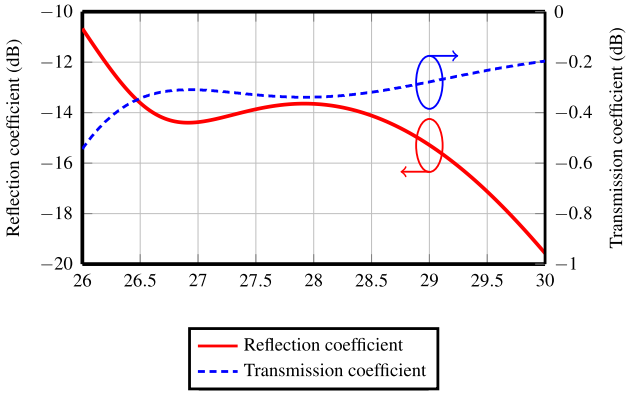


**FIGURE 6.** Simulated transition reflection and transmission coefficients without phase shifter.

The simulated S-parameters with the optimized transition values and without the phase shifter in between the transitions are shown in Fig. 6. The S-parameter results include both transitions combined and confirm the reflection coefficient is below $-10$ dB for the whole band and the transmission coefficient is mostly above $-0.4$ dB.

### C. PHASE SHIFTERS AND PCB DESIGN

Element phases are controlled with 5-bit TGP2100 phase shifters from Qorvo designed to operate at 28–32 GHz [26]. The phase shifter in question is of digital type with 32 phase shifter states nominally offset by 11.25° discrete steps. Each phase shifter requires six digital dc-voltage lines (0 V or 5 V) to control the component. One is used for biasing the phase shifter and other five are utilized to determine the phase state.

The bottom of the phase shifter chip provides its dc- and RF-ground. Because of this, there is a milled cavity for the phase shifter so it can be mounted directly to the PCB ground plane. RF-signal pads and the control-voltage pads on the

phase shifter are wirebonded to corresponding lines on the PCB. Thus there should be enough space above the phase shifter and the PCB for the bondwires. The available space for the phase shifters is determined by the element spacing i.e. the horn antenna aperture size. The height of both waveguides are tapered around the PCB to have more space for the phase shifter. For similar reasons the adjacent waveguides share their boundary walls with each other.

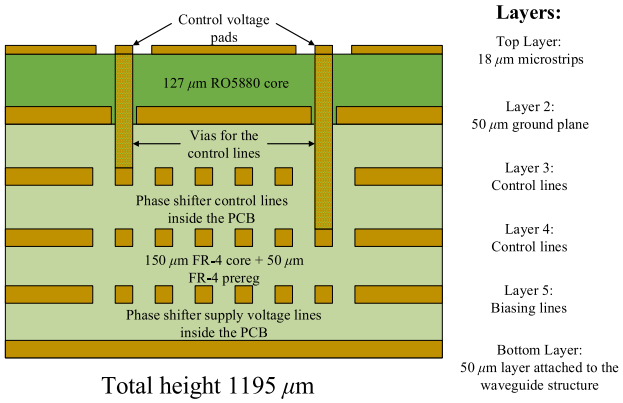


**FIGURE 7.** PCB outline from the side presenting the different layers.

Careful PCB design is required to ensure the proper transition performance and to control the phase shifter. Fig. 7 presents the design. Multi-layer PCB is designed to work in the following way: the 1st i.e. the top layer is where the transition microstrip lines are located and where the wirebonding for the phase shifter is done. The 2nd layer is the ground plane for the microstrip line and phase shifter is directly attached to the plane. The 3rd and 4th layers have routing for the control voltages of the phase shifters i.e. they are called control layers. They are designed so that one layer provides control for two antenna columns as there is not enough space for all the control lines in one layer. The 5th layer has routing for the biasing voltages and is called biasing layer. The 6th i.e. the bottom layer is attached to the waveguide structure.

The PCB structure is scalable: by increasing the number of layers, the number of antenna columns can be increased as each new control layer provides the control lines for two new antenna columns and the supply layer can support multiple columns. Antenna rows can be simply increased by increasing the physical size of the PCB as in that direction there are no limitations for the control line routing.

The simulated reflection and transmission coefficient results when the phase shifter is added in between the transitions are presented in Fig. 8a and 8b. The phase shifter S-parameters are provided by the manufacturer and they show that the reflection and the transmission are dependent on the used phase shifter state. In Fig. 8a and 8b the area on which the coefficients vary are highlighted. In addition, the average coefficient values of the phase shifter states and transitions are shown with the average values obtained from the phase shifter states. The bond wires are also included in

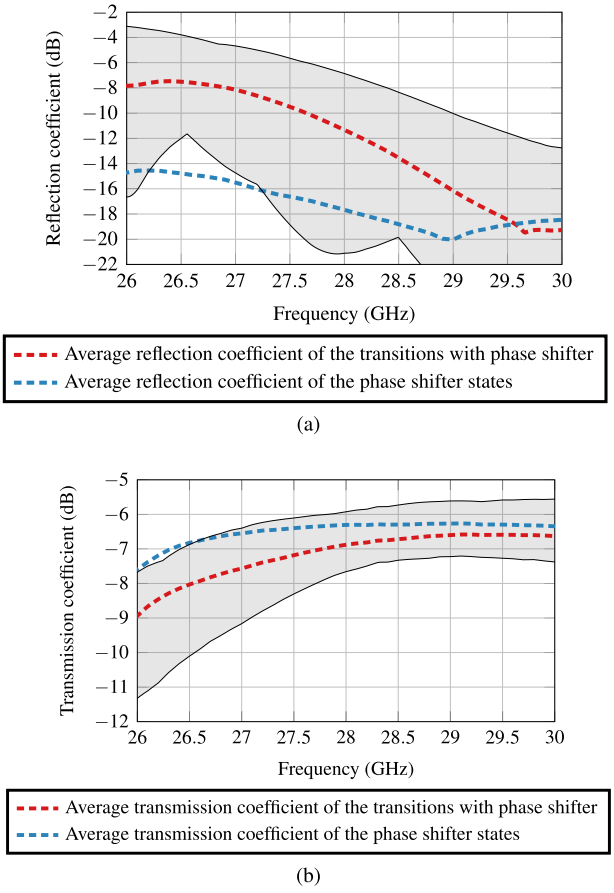


**FIGURE 8.** Simulated reflection and transmission coefficients of both transitions and the phase shifter with bond wires: (a) reflection and (b) transmission coefficient. The variation for all the phase shifter states is highlighted.

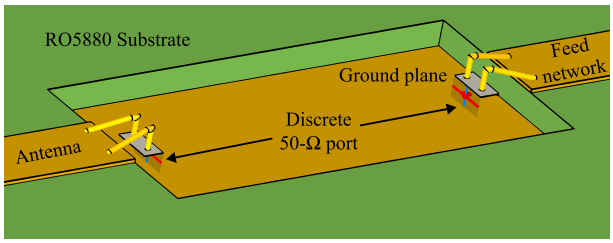


**FIGURE 9.** CST-simulation model illustrating the discrete 50-Ω ports to which the S-parameter presentations of the phase shifter states are connected.

the CST-simulation model (see Fig. 9): they are gold wires with a diameter of 25 $\mu$m. In simulations their height is 0.1 mm and they are connected to a ground plane of the PCB with discrete 50-Ω ports.

Simulation results show that the main losses in the transition are due to the phase shifters. Especially transmission coefficient results clearly show how the transmission losses with the phase shifter are more than 6.5 dB when compared to the results without the phase shifter. Furthermore, the matching is poorer at the lower frequencies of the chosen band which is expected as the main operation range of the phase

shifter is from 28 GHz to 32 GHz. In addition, the bond wires are not perfectly matched which increases the reflections. The phase shifter losses would be overcome by using the phase shifting functionality in conjunction with active components, such as those used in [15], [16].

### D. HORN ANTENNA ARRAY

The array is constructed from pyramidal horn antenna elements in 4 by 4 configuration. The aperture size of a single element is 7.8 mm in both E- and H-planes. The maximum gain of the lossless 16-element array can be expected to be 20.4 dBi towards broadside. In reality, the realized gain of the array can be expected to be considerably less. As shown in Fig. 8b, the average transmission losses due to phase shifters and transitions are 7 dB. Addition to that, there will be ohmic losses in waveguide structures and losses due to the surface roughness in microstrip lines. Thus, it is reasonable to expect the realized gain to be around 11.0–12.5 dBi towards broadside at 28 GHz.

Furthermore, due to the large element spacing (7.9 mm which corresponds to 0.74$\lambda$ at 28 GHz) the grating lobes can be expected to rise quite fast when the main beam is steered: already after 20° beam steering according to simulations. However, it is impossible to reduce element spacing as the aperture dimension in H-plane is dictated by the cut-off frequency of the waveguide.

## III. MEASUREMENTS

The far-field pattern of the antenna is acquired from the planar near-field measurements that are done using an open-ended WR-28 waveguide as a near-field measurement probe. Furthermore, the near-field measurement software makes the probe correction to the measurement results so that the effect of the measurement probe is not affecting the far-field pattern. The measurement cable is connected to the antenna under test with the R281A coaxial-to-waveguide transition connector. The R281A S-parameters are also measured verifying negligible reflection and insertion losses. Thus, it does not affect the antenna performance.

Antenna beam is steered in elevation, azimuth, and diagonal directions. Broadside is defined to be at 0° and the steering angle can be both negative and positive. Antenna beam steering is done based on the simulation results: the initial phase of each element is taken from the simulations at the center frequency 28 GHz, and element 1, see Fig. 1, is used as a reference element against which the other element phases are adjusted.

### A. BEAM-CONTROL EQUIPMENT

The phase shifters are controlled using NI-USB 6509 DAQ-device with R100-50-50 cable. The device outputs 100 signal lines which are divided by the cable to the two 50-pin connectors. The output is 0 V or +5 V voltage for each line.

The device is controlled using Data Acquisition Toolbox in MATLAB. Six signal lines are required to control each phase shifter and corresponding digital channels are programmed with MATLAB so that each phase shifter can be controlled with similar commands.

### B. BEAM-STEERING MEASUREMENTS

First, the field intensity of the antenna aperture is calculated from the measured near-field data. The produced hologram image is evaluated to inspect that all the elements are working as intended. The field intensity is very low on the lower left corner as seen in Fig. 10, which shows that element number 13 does not work. Since the element in question is a corner one, its malfunctioning does not result into grating lobes but only decreases the overall gain. According to the simulations, the defective element lowers the gain by 0.3 dB which is consistent with the array theory.

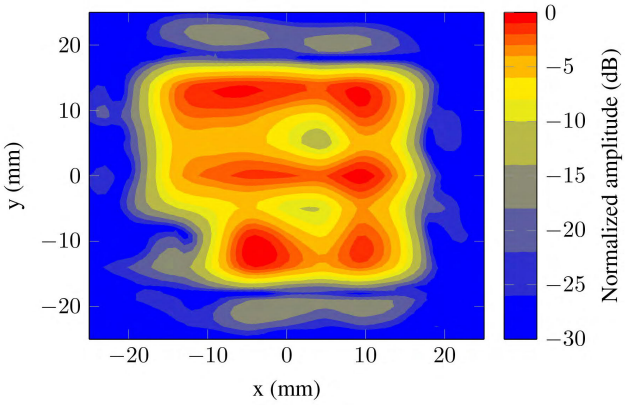


**FIGURE 10.** Measured field intensity at the antenna aperture with broadside beam at 28 GHz.

Further evaluations suggest that the problem with the element 13 is related to the phase shifter and the PCB. Additional near-field measurements have also been conducted of the antenna structure without the PCB in place i.e., the power division network waveguides are directly connected to the antenna elements. The results show that power is received through every element and the power division network is working as intended. Furthermore, the similar field intensity results for the other elements can be acquired by turning off their corresponding phase shifters, meaning that the bias voltage is not fed to them. However, it is not certain where the problem is exactly: malfunction in element 13 can be due to PCB with broken bias or control lines, defective phase shifter, or broken or faulty bond wire.

The measurements show that the beam steering works as intended and the realized gain of the antenna is 10.7 dBi towards broadside, which is reasonable when taking into account the transmission losses and the defective element. Furthermore, the gain measurement uncertainty is few tenths of decibel, as the gain is determined by the gain comparison using a reference horn antenna. The beam steering in azimuth direction is shown in Fig. 11 and in elevation direction in Fig. 12. In both directions the steering is shown from +20° to −30° to demonstrate steering in all directions. Due to small

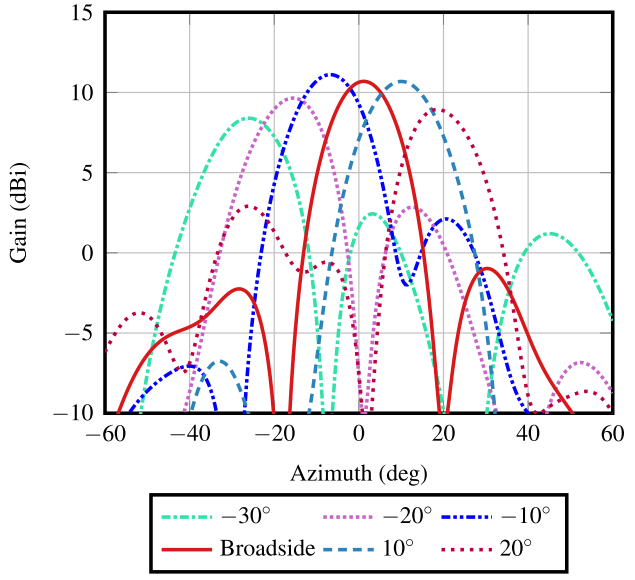


**FIGURE 11.** Measured beams in azimuth direction at 28 GHz.

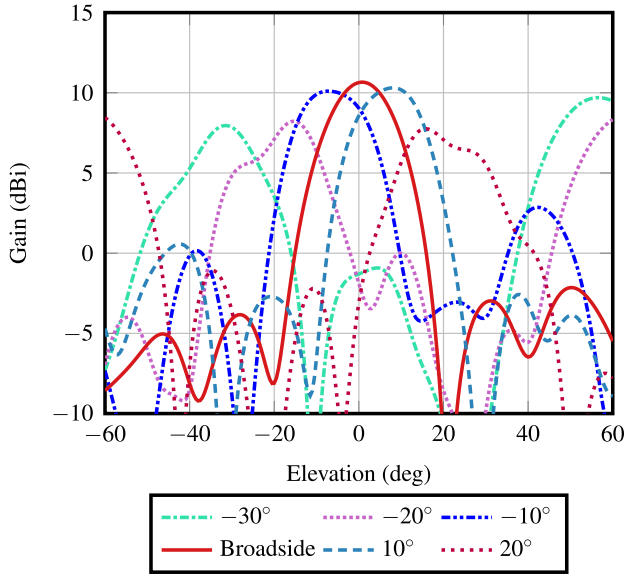


**FIGURE 12.** Measured beams in elevation direction at 28 GHz.

mutual coupling between the elements, the beam does not steer as much as it would with an ideal array. However, beam could be steered even more using other than progressive phase coefficients. Further, the beam shape with elevation steering does not stay fully coherent and the grating lobes rise earlier than compared to the azimuth steering. As suggested by the simulations the grating lobes start to rise after ±20° steering angles which can especially be seen in the elevation gain patterns. The realized gain of the antenna can also be seen varying with the beam-steering angle but this is expected as some power is lost to the rising side lobes.

The measured and simulated reflection coefficients of the antenna system are presented in Fig. 13, for the

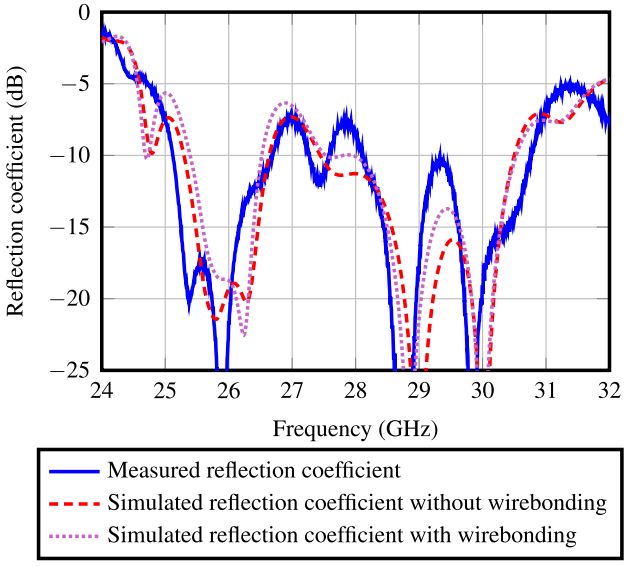


**FIGURE 13.** Comparison of the measured and simulated antenna reflection coefficients with broadside beam.

broadside beam. These results show good overall agreement between the simulations and the measurements. The simulated reflection coefficients are shown both with the wirebonding and without it. This is done to demonstrate the effect of the wirebonding, which slightly deteriorates the matching. Differences between the simulations and measurements can be explained with the uncertainty of the bond wires: each wire differs slightly in length and landing positions and they are not identical as in the simulations.

**TABLE 2.** Simulated and measured (uncalibrated) antenna characteristics for different beam-steering angles at 28 GHz.

| PCB | Angle(°) | Realized Gain sim./meas. (dBi) (uncalibrated) | 3 dB angular width sim./meas. |
|---|---|---|---|
| Broadside | | 12.3/10.7 | 16.7°/16.5° |
| Elevation plane | 10 | 11.6/10.4 | 16.7°/18.5° |
| | 20 | 8.7/7.8 | 20.2°/23.5° |
| | −10 | 11.4/10.2 | 16.7°/20.0° |
| | −20 | 8.6/8.4 | 19.7°/21.0° |
| | −30 | 8.3/8.0 | 21.2°/18.5° |
| Azimuth plane | 10 | 12.1/10.7 | 17.4°/19.0° |
| | 20 | 11.0/9.0 | 17.5°/18.0° |
| | −10 | 12.0/11.1 | 17.3°/18.0° |
| | −20 | 11.1/9.7 | 17.7°/18.5° |
| | −30 | 10.0/8.4 | 18.2°/20.0° |

Table 2 shows the comparison between the simulated and measured antenna characteristics. The simulated values take into account the wirebonding. The measured realized gain results are in all cases slightly less than the simulated ones. The lower gain can be explained with the uncertainty in the phase shifter operation, the wirebonding, material and surface roughness losses at 28 GHz, and the initial phase of each element. Based on these measured and simulated results, and considering the matching losses, defective element, and

measurement uncertainties, it is fair to assume that the losses due to waveguide structure are no more than 1 dB.

### C. ELEMENT PHASE CALIBRATION

The phase of each element is calibrated at 28 GHz. Calibration is worthwhile as the phase shifter may have some phase error over the evaluated frequency band. The initial phase of each element is measured using near field scanner right in front of the element in question while the other elements are turned off. These results provide the initial phase from the feed network without any phase shifting. The measurement results are then used to calculate the required phase shifts for each beam-steering angle. The effect of the antenna calibration is shown in Fig. 14 for the broadside beam.

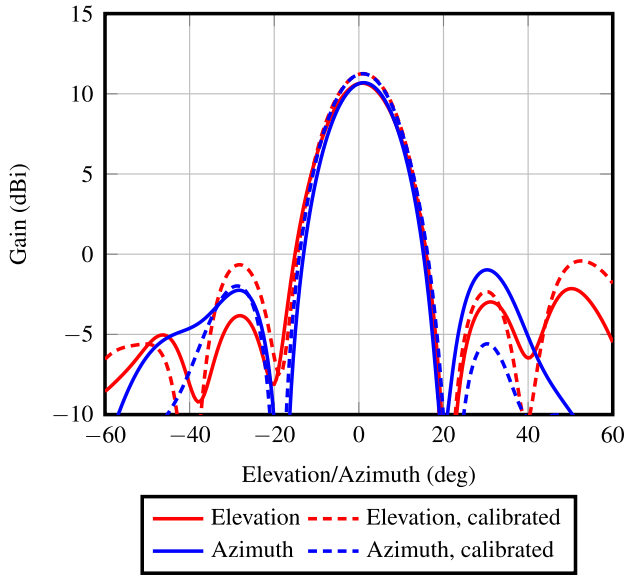


**FIGURE 14.** Effect of the antenna calibration in broadside at 28 GHz.

There is a slight increase in the realized gain of $\approx 0.6$ dB due to the calibration, resulting the 11.3 dBi gain. The measured results indicate that the simulated results of the initial phase are quite accurate. Most of the phase shifters require state change of 1 or 2 steps from the values that are optimal in the simulations. However, at other beam-steering angles the calibration could potentially provide significant increase in the measured gain and decrease sidelobe level. Further calibrations would require the phase measurements of the each element with every possible phase state at each frequency. These results could then be utilized to realize optimal beamforming for each steering angle. Furthermore, active impedance of each element depends on the beam-steering angle. Active impedance variations could be mitigated with the phase shifters to some extent.

## IV. DISCUSSION

The results show that the designed phased-array antenna operates well and that the concept could be used to realize millimeter-wave access or backhaul in base stations. However, there are still some issues to be solved before the antenna could be taken into commercial use.

Milling the antenna from brass is not ideal manufacturing method for mass production. Plastic injection molding or 3D printing with metal coating might be possible solutions. We verified with the commercial manufacturer that the current antenna structure can be manufactured in stereolithography 3D printing process followed by metal plating. Plastic injection molding has also been proved to be possible way to produce millimeter-wave antennas [27].

The measured reflection coefficient peaks above $-10$ dB between 26.5–28.5 GHz for the broadside beam. The transitions have been designed without the phase shifter in between them i.e. they have been replaced by the microstrip line. The matching could be improved significantly by taking into account the phase shifter already in the transition design. Finally, the matching of the bond wires could be improved – we learned after the PCB-manufacturing that in order to compensate the inductance of the bond wires, larger pads would be required at the end of the microstrip lines from which the wires are bonded to the chip.

The grating lobes arise already at relatively small steering angles because of relatively large element spacing. The current spacing is dictated by the cut-off frequency of the waveguide which affects its size in H-plane. The spacing is kept the same in E-plane due to the symmetry and so that the phase shifters have enough space for mounting them. The element spacing could be reduced for example with dielectric filling inside the waveguides to scale down their dimensions. Of course, as a trade-off this would introduce more losses.

The prototype has relatively low gain for 5G networks but the number of the elements in the realized array could be scaled up to result in higher gain. Increasing the element number would necessitate redesigning the feed network, which is relatively straightforward especially for the primary network. In addition, the proposed PCB design supports scalability up for several rows of the array. However, the large number of control lines needed would first limit increasing the element number massively. Each antenna element necessitates 6 control lines, which are challenging to fit. This issue might be solved by using microcontrollers to control subsets of phase shifters.

The utilized phase shifters also set challenges in real applications. The phase shifter losses are too high at the moment to be used in a realizable 5G antenna array. Instead, the array would require additional amplifiers or vector modulator based phase shifters with active gain in order to compensate the losses. Active IC elements might require cooling. It could be possible to realize the horn antenna part from metal, in which case it might passively radiate the heat out. However, even with the lossy phase shifters, the losses in the presented solution are far less inferior compared to the existing solutions where the similar structure would be implemented on the PCB, as the waveguide structures provide very low losses.

## V. CONLUSIONS

A scalable, beam-steerable phased antenna array for future 5G wireless backhaul communications is designed, manufactured, and measured. The antenna provides ±20° grating-lobe free beam-steering range both in elevation and azimuth. The measured realized gain at 28 GHz is 11.3 dBi towards broadside direction and the measurement results are well in line with the simulation results. The maximum gain of the lossless array would be 20.4 dBi and the simulations show that the average losses due to phase shifters and transitions are already 7 dB. After taking into account the matching losses, defective element, and measurement uncertainties, it is fair to assume that the losses due to waveguide structure are no more than 1 dB in the measured antenna. These are very low-losses compared to the planar antenna realizations at millimeter-wave frequencies.

The antenna structure itself exhibits very low losses and majority of the losses are caused by the phase shifter. To the authors' knowledge this is the first realization of an antenna where a low-loss waveguide power division network and antenna elements are integrated with PCB-mounted element-specific phase shifters, which can be controlled electronically and in real time. The prototype has proven that this kind of antenna array could potentially be feasible for future 5G communications and these preliminary results are very promising. The concept is clearly an option for the future 5G networks.

## ACKNOWLEDGMENT

The authors would like to thank Dr. Md. Mazidul Islam for the discussions related to the antenna transformation from the E-band and the PCB fabrication, Mr. Eino Kahra for the help with the antenna fabrication, and Mr. Samu Pälli for carrying out antenna measurements.

## REFERENCES

[1] "Cisco visual networking index: Forecast and trends, 2017–2022," Cisco Syst., San Jose, CA, White Paper C11-741490-00, Feb. 2019.
[2] M. Agiwal, A. Roy, and N. Saxena, "Next generation 5G wireless networks: A comprehensive survey," *IEEE Commun. Surveys Tuts.*, vol. 18, no. 3, pp. 1617–1655, 3rd Quart., 2016.
[3] "5G new radio network," Nokia, Espoo, Finland, White Paper SR1803023634EN, Apr. 2018.
[4] "From today to tomorrow, Huawei microwave & mm–Wave whitepaper," Huawei Technol., Shenzhen, China, White Paper EDOC1000097991, Mar. 2016.
[5] "5G radio access," Ericsson, Stockholm, Sweden, White Paper UEN 28423-3204 Rev C, Apr. 2016.
[6] J. G. Andrews, S. Buzzi, W. Choi, S. V. Hanly, A. Lozano, A. C. K. Soong, and J. C. Zhang, "What will 5G be?" *IEEE J. Sel. Areas Commun.*, vol. 32, no. 6, pp. 1065–1082, Jun. 2014.
[7] M. Shariat, M. Dianati, K. Seppänen, T. Suihko, J. Putkonen, and V. Frascolla, "Enabling wireless backhauling for next generation mmWave networks," in *Proc. Eur. Conf. Netw. Commun. (EuCNC)*, Jun. 2015, pp. 164–168.
[8] A. F. Molisch, *Wireless Communications*. 2nd ed. Chichester, U.K.: Wiley, 2011.
[9] J. Ala-Laurinaho, J. Aurinsalo, A. Karttunen, M. Kaunisto, A. Lamminen, J. Nurmiharju, A. V. Räisänen, J. Säily, and P. Wainio, "2-D beam-steerable integrated lens antenna system for 5G E-band access and backhaul," *IEEE Trans. Microw. Theory Techn.*, vol. 64, no. 7, pp. 2244–2255, Jul. 2016.
[10] Y. J. Cheng, W. Hong, K. Wu, Z. Q. Kuai, C. Yu, J. X. Chen, J. Y. Zhou, and H. J. Tang, "Substrate integrated waveguide (SIW) Rotman lens and its Ka-band multibeam array antenna applications," *IEEE Trans. Antennas Propag.*, vol. 56, no. 8, pp. 2504–2513, Aug. 2008.
[11] D. Sánchez-Escuderos, M. Ferrando-Bataller, J. I. Herranz, and M. Cabedo-Fabrés, "Periodic leaky-wave antenna on planar Goubau line at millimeter-wave frequencies," *IEEE Antennas Wireless Propag. Lett.*, vol. 12, pp. 1006–1009, 2013.
[12] K. K. Karnati, M. E. Trampler, and X. Gong, "A monolithically BST-integrated Ka-band beamsteerable reflectarray antenna," *IEEE Trans. Antennas Propag.*, vol. 65, no. 1, pp. 159–166, Jan. 2017.
[13] T. Chaloun, W. Menzel, F. Tabarani, T. Purtova, H. Schumacher, M. Kaynak, Q. Luo, S. Gao, R. Starec, and V. Ziegler, "Wide-angle scanning active transmit/receive reflectarray," *IET Microw., Antennas Propag.*, vol. 8, no. 11, pp. 811–818, Aug. 2014.
[14] N. Ojaroudiparchin, M. Shen, and G. F. Pedersen, "8×8 planar phased array antenna with high efficiency and insensitivity properties for 5G mobile base stations," in *Proc. 10th Eur. Conf. Antennas Propag. (EuCAP)*, Apr. 2016, pp. 1–5.
[15] K. Kibaroglu, M. Sayginer, T. Phelps, and G. M. Rebeiz, "A 64-element 28-GHz phased-array transceiver with 52-dBm EIRP and 8-12-Gb/s 5G link at 300 meters without any calibration," *IEEE Trans. Microw. Theory Techn.*, vol. 66, no. 12, pp. 5796–5811, Dec. 2018.
[16] R. Valkonen, "Compact 28-GHz phased array antenna for 5G access," in *IEEE/MTT-S Int. Microw. Symp.*, Jun. 2018, pp. 1334–1337.
[17] T. Sehm, A. Lehto, and A. V. Räisänen, "A high-gain 58-GHz box-horn array antenna with suppressed grating lobes," *IEEE Trans. Antennas Propag.*, vol. 47, no. 7, pp. 1125–1130, Jul. 1999.
[18] D. Kim, M. Zhang, J. Hirokawa, and M. Ando, "Design and fabrication of a dual-polarization waveguide slot array antenna with high isolation and high antenna efficiency for the 60 GHz band," *IEEE Trans. Antennas Propag.*, vol. 62, no. 6, pp. 3019–3027, Jun. 2014.
[19] D. Zarifi, A. Farahbakhsh, and A. U. Zaman, "A gap waveguide-fed wideband patch antenna array for 60-GHz applications," *IEEE Trans. Antennas Propag.*, vol. 65, no. 9, pp. 4875–4879, Sep. 2017.
[20] F. Xu, K. Wu, and X. Zhang, "Periodic leaky-wave antenna for millimeter wave applications based on substrate integrated waveguide," *IEEE Trans. Antennas Propag.*, vol. 58, no. 2, pp. 340–347, Feb. 2010.
[21] Y. J. Cheng and Y. Fan, "Millimeter-wave miniaturized substrate integrated multibeam antenna," *IEEE Trans. Antennas Propag.*, vol. 59, no. 12, pp. 4840–4844, Dec. 2011.
[22] M. M. Islam, M. Leino, R. Luomaniemi, J. Song, R. Valkonen, J. Ala-Laurinaho, and V. Viikari, "E-band beam-steerable and scalable phased antenna array for 5G access point," *Int. J. Antennas Propag.*, vol. 2018, Nov. 2018, Art. no. 4267053.
[23] T. Sehm, A. Lehto, and A. V. Räisänen, "A large planar 39-GHz antenna array of waveguide-fed horns," *IEEE Trans. Antennas Propag.*, vol. 46, no. 8, pp. 1189–1193, Aug. 1998.
[24] Y.-C. Shih, T.-N. Ton, and L. Q. Bui, "Waveguide-to-microstrip transitions for millimeter-wave applications," in *IEEE MTT-S Int. Microw. Symp. Dig.*, May 1988, pp. 473–475.
[25] T. Q. Ho and Y.-C. Shih, "Spectral-domain analysis of E-plane waveguide to microstrip transitions" *IEEE Trans. Microw. Theory Techn.*, vol. 37, no. 2, pp. 388–392, Feb. 1989.
[26] Qorvo. (Apr. 2019). *TGP2100 30 GHz 5-Bit Digital Phase Shifter*. TGP2100 datasheet. Accessed: May 2019. [Online]. Available: https://www.qorvo.com/products/p/TGP2100
[27] R. Dolp, W. Mayer, and W. Grabherr, "Industrialization of a 58 GHz high gain flat panel antenna design using injection molding technique," in *Proc. 29th Eur. Microw. Conf.*, Oct. 1999, pp. 13–15.

**MIKKO K. LEINO** (S'16) was born in Espoo, Finland, in 1990. He received the B.Sc. (Tech.) and M.Sc. (Tech.) (Hons.) degrees in electrical engineering from Aalto University, Espoo, Finland, in 2016 and 2017, respectively, where he is currently pursuing the D.Sc. (Tech.) degree.

From 2015 to 2017, he was a Research Assistant with Aalto University. Since 2017, he has been a Doctoral Candidate with the Department of Electronics and Nanoengineering, School of Electrical Engineering, Aalto University. His current research interest includes beam-steerable millimeter-wave antennas and their characterization.

Mr. Leino was a recipient of the second price in the IEEE Antennas and Propagation Society 2016 Student Design Contest, in 2016.

**RESTI MONTOYA MORENO** was born in Albacete, Spain, in 1992. He received the B.Sc. (Tech.) degree in telecommunications engineering from the Universitat Politècnica de València, in 2014, and the M.Sc. (Tech.) degree (Hons.) in electrical engineering from Aalto University, Espoo, Finland, in 2016, where he is currently pursuing the D.Sc. (Tech.) degree.

He was a Research Assistant with Aalto University, before joining Intel as an RF Engineer Intern, in 2016. Since 2017, he has been a Doctoral Candidate with the Department of Electronics and Nanoengineering, School of Electrical Engineering, Aalto University. His current research interest includes 5G and mm-wave antennas for base stations and mobile devices.

**JUHA ALA-LAURINAHO** received the Diploma Engineer (M.Sc.) degree in mathematics and D.Sc. (Tech.) degree in electrical engineering from the TKK Helsinki University of Technology, Finland, in 1995 and 2001, respectively.

He has been with the TKK, currently Aalto University, serving in the Radio Laboratory in 1995–2007, in the Department of Radio Science and Engineering in 2008–2016, and currently in the Department of Electronics and Nanoengineering. During 1995, he worked as a Research Assistant and, since 1996, he has been a Research Associate and currently he works as a Staff Scientist. Dr. Ala-Laurinaho has been a Project Manager in many millimeter-wave technology related projects. His current research interests are the antennas and antenna measurement techniques for millimeter and submillimeter waves, and the millimeter-wave imaging.

**RISTO VALKONEN** received the M.Sc. (Tech.) degree in communications engineering and the D.Sc. (Tech.) degree in electrical engineering from Aalto University, Finland, in 2007 and 2013, respectively.

From 2006 to 2013, he was with the Department of Radio Science and Engineering, Aalto University. From 2013 to 2015, he was Postdoctoral Researcher with the University of Kiel. Since 2015, he has been with Nokia and since 2016 with Nokia Bell Labs as Antenna Specialist. His research interest includes antennas and RF front-ends for future communication systems.

**VILLE VIIKARI** (S'06–A'09–M'09–SM'10) was born in Espoo, Finland, in 1979. He received the M.Sc. (Tech.) and D.Sc. (Tech.) (Hons.) degrees in electrical engineering from the Helsinki University of Technology (TKK), Espoo, Finland, in 2004 and 2007, respectively.

From 2001 to 2007, he was with the Radio Laboratory, TKK, where he studied antenna measurement techniques at submillimeter wavelengths and antenna pattern correction techniques. From 2007 to 2012, he was a Research Scientist and a Senior Scientist with the VTT Technical Research Centre, Espoo, where his research included wireless sensors, RFID, radar applications, MEMS, and microwave sensors. He is currently an Associate Professor and the Deputy Head of the Department with the School of Electrical Engineering, Aalto University, Espoo, Finland. His current research interests include antennas for mobile networks, RF-powered devices, and antenna measurement techniques.

Dr. Viikari has served as the Chair of the Technical Program Committee of the ESA Workshop on Millimetre-Wave Technology and Applications and the Global Symposium on Millimeter Waves (GSMM) twice, in Espoo, Finland, in 2011 and 2016, respectively. He was a recipient of the Young Researcher Award (2014), presented by the Finnish Foundation for Technology Promotion, the IEEE Sensors Council 2010 Early Career Gold Award, the 2008 Young Scientist Award of the URSI XXXI Finnish Convention on Radio Science, Espoo, Finland, and the Best Student Paper Award of the Annual Symposium of the Antenna Measurement Techniques Association, Newport, RI, USA (2005).